RSC Advances

PAPER

View Article Online
View Journal | View Issue

Cite this: *RSC Adv.*, 2023, **13**, 3425

Preparation and self-assembly of ionic (PNIPAM-*co*-VIM) microgels and their adsorption property for phosphate ions†

Jianping Yang,*[a] Bei Huang,[b] Zhengxiang Lv[a] and Zheng Cao *[bc]

Using *N*-isopropyl acrylamide (NIPAM) as the main monomer, 1-vinyl imidazole (VIM) containing tertiary amine groups as the functional comonomer, and 1,5-dibromo pentane as the crosslinking agent, ionic P(NIPAM-*co*-VIM) microgels were prepared by a two-step method. The crosslinking agent was reacted with tertiary amino groups by the quaternary amination. The results of zeta potential and particle size analysis showed that P(NIPAM-*co*-VIM) microgels were positively charged and had a particle size of about 400 nm, and the microgels with 11 wt% VIM still showed temperature sensitivity with a volume phase transition temperature of approximately 37.5 °C. The effects of VIM content, ambient temperature, and pH on the adsorption properties of the microgels for phosphate anions were explored. The self-assembly of the positively charged P(NIPAM-*co*-VIM) microgels with polyelectrolytes and the adsorption behavior of the layers for phosphate anions were studied using a quartz crystal microbalance (QCM). It was found that at a phosphate concentration of 0.3 mg mL^{-1}, VIM mass fraction of 11%, pH of 5, and temperature of 20 °C, the largest adsorption capacity of P(NIPAM-*co*-VIM) microgel on phosphate ions could reach 346.3 mg g^{-1}. The frequency responses of the microgel-modified QCM sensor could reach 3.0, 18.8, and 25.9 Hz when exposed to 10^{-8}, 10^{-7}, and 10^{-6} M phosphate solutions. Therefore, the ionic (PNIPAM-*co*-VIM) microgels could be promising for fabricating anion-binding materials for separation and sensing applications.

Received 22nd October 2022
Accepted 9th January 2023

DOI: 10.1039/d2ra06678e

rsc.li/rsc-advances

1 Introduction

A microgel is a kind of polymer with a size of 50–5000 nm and a crosslinked network structure. It is easy to introduce functional groups into a microgel, and it has a large specific surface area and fast environmental response performance.[1–7] Currently, there are many studies on environmentally sensitive microgels, which can change physically or chemically with a change in the external environment. According to different external influence factors, environmentally sensitive microgels can be divided into temperature-responsive microgels, magnetic-responsive microgels, pressure-responsive microgels, near-infrared laser-responsive microgels, pH-responsive microgels, and multi-responsive microgels.[8–16] Nowadays, microgels have many applications in dye and ion sensing and adsorption, such as selective adsorption of metal ions, such as Ni^{2+}, Cu^{2+}, Co^{2+}, Pb^{2+}, and dye molecules,[17–24] but there are few reports on the adsorption of phosphate ions.[25,26] Phosphorus discharged into water can easily lead to eutrophication, and phosphorus-containing wastewater discharged into soil will cause soil zinc deficiency. Phosphorus mainly exists in the form of phosphate ions in a water environment. Therefore, it is of great significance to develop efficient microgel adsorption materials and to remove excessive phosphate ions from water.[27,28]

Hui *et al.*[29] prepared polyvinyl alcohol hydrogel microspheres containing aluminum ions (Al^{3+}) in a internal network structure by a chemical crosslinking method. It was found that with an increase in $AlCl_3$ concentration and an extension of crosslinking time, the permeability of the hydrogel decreased, and the adsorption capacity for phosphate ions first increased and then decreased. Liu *et al.*[30] prepared zirconium(IV)-loaded crosslinked chitosan particles (CCP-Zr) by a membrane forming and crosslinking method, and studied their adsorption properties for phosphate ions. The adsorption mechanism was attributed to the electrostatic interaction and ion exchange

[a]*Department of Orthopedics, Changzhou Hospital of Traditional Chinese Medicine, 25 Heping North Road, Changzhou, 213000, Jiangsu, P. R. China. E-mail: 43655304@qq.com*

[b]*Jiangsu Key Laboratory of Environmentally Friendly Polymeric Materials, School of Materials Science and Engineering, Jiangsu Collaborative Innovation Center of Photovoltaic Science and Engineering, Changzhou University, Changzhou 213164, Jiangsu, P. R. China. E-mail: zcao@cczu.edu.cn*

[c]*National Experimental Demonstration Center for Materials Science and Engineering (Changzhou University), Changzhou, 213164, P. R. China*

† Electronic supplementary information (ESI) available: Visual appearance of blank solution and phosphomolybdate blue solutions prepared (Fig. S1) and the standard work curve (Fig. S2). The composition and molecular weights (M_w) of copolymers (Table S1). The particle size of the final swelling microgels as a function of pH (Fig. S3). See DOI: https://doi.org/10.1039/d2ra06678e

reaction between CCP-Zr and phosphate ions. Using *N*-isopropyl acrylamide (NIPAM) as the main monomer and *N*-allyl thiourea (ATU) as the functional comonomer, Chen *et al.*[31] prepared thermosensitive P(NIPAM-*co*-ATU) microgels by free radical polymerization. Due to the strong adsorption of thiourea groups and phosphate ions, the adsorption capacity of P(NIPAM-*co*-ATU) microgels for phosphate ions can reach 91 mg g^{-1}. It can be seen that an adsorption method based on microgel particles or microspheres is a suitable method for treating low-content pollutants in solution. It has the advantages of simple operation, low cost, and high efficiency, and has become a research hotspot at home and abroad. The functional groups on the microgel network structure can adsorb phosphate ions by electrostatic interaction. It is very important to find and develop microgel materials that can strongly adsorb phosphate ions and realize the adsorption and separation of phosphate ions.

In recent years, environmentally responsive ionized microgels have attracted more and more attention and are expected to be ideal materials for the adsorption and separation of phosphate ions. Using *N*-isopropyl acrylamide (NIPAM) as the main monomer and 1-vinyl imidazole (VIM) or 4-vinyl pyridine (4VP) as the comonomer, Zhou *et al.*[32] successfully obtained a thermosensitive ionic microgel with narrow distribution by *in situ* quaternization crosslinking *via* soap-free emulsion polymerization. As crosslinking agents, 1,4-dibromobutane and 1,6-dibromohexane are quaternized with tertiary amine groups in the copolymer to form a crosslinked network and thermosensitive ionic microgels. In addition, the ionic microgels showed good encapsulation and release ability for anionic dyes (such as methyl orange, MO). However, there are few applications for the adsorption and separation of phosphate ions by such ionic microgels. It is considered that microgels can be functionalized by ion exchange, the design of crosslinking agents with new structures, and further quaternization. They can be applied to treatment of dye wastewater, degradable templates, metal ion detection, and other fields.[33–35] In addition, there is an urgent need for real-time detection and efficient technical means to facilitate the study of the interaction between ionized microgels and phosphate ions, and to provide a reference for the better development of adsorption and sensing materials for phosphate ions. A quartz crystal microbalance (QCM) is a powerful tool for detecting the mass change of a trace material on the surface of the quartz crystal sensor, with high detection sensitivity, easy surface modification, real-time detection, and other advantages, and it has been widely used in polyelectrolyte self-assembly,[36–38] protein or enzyme adsorption,[39,40] chain conformation,[41,42] chemical sensors,[43–47] and biodegradation[48] and other fields. In this work, *N*-isopropyl acrylamide (NIPAM) was used the main monomer, and 1-vinyl imidazole (VIM) was added as a functional copolymer monomer to prepare a temperature-sensitive P(NIPAM-*co*-VIM) microgel, and its structure, properties, and ability to adsorb phosphate ions were studied. At the same time, the layer-by-layer (LbL) self-assembly behavior of the charged and ionized microgels and the oppositely-charged polyelectrolytes driven by electrostatic forces was studied by QCM technology, and the self-assembled microgels were used as sensing coatings for QCM, and the adsorption interaction between microgels and phosphate ions was studied. The addition of functional monomer VIM is expected to improve the capacity of the microgel to adsorb phosphate ions and to develop high-efficiency phosphate ion adsorption materials.

2 Experimental

2.1 Chemicals and materials

1-Vinyl imidazole (VIM, ≥98%), *N*-isopropyl acrylamide (NIPAM, ≥99%), 2,2′-azoisobutyronitrile (AIBN, ≥98%), 1,4-dioxane (DOA, ≥99%), 1, 5-dibromopentane (DMP, ≥97%), polyethyleneimine (PEI, branched, M_w = 10 000, ≥99%), sodium polystyrene sulfonate (PSS, ≥99%), potassium persulfate (≥99%), and *N*,*N*′-methylenebis(acrylamide) (MBA, ≥98%) were all purchased at J & K Chemical Co., Ltd. (Beijing, Shanghai). Ascorbic acid ($C_6H_8O_6$, ≥99%) and potassium antimony tartrate (≥99%) were obtained from Sinopharm Group Chemical Reagent Co., Ltd. Ammonium molybdate tetrahydrate ($(NH_4)_6MO_7O_{24}\cdot 4H_2O$, ≥99%) was bought from Shanghai Shenbo Chemical Co., Ltd. Potassium dihydrogen phosphate (KH_2PO_4, ≥99%) was obtained from Yonghua Chemical Technology Co., Ltd. (Suzhou, China). Sodium phosphate dodecahydrate ($Na_3PO_4\cdot 12H_2O$, ≥99%) was purchased from Jiangsu Qiangsheng Chemical Co., Ltd. (Changshu, China).

2.2 Preparation of ionic P(NIPAM-*co*-VIM) microgels

P(NIPAM-*co*-VIM) microgels were synthesized by a two-step method. The P(NIPAM-*co*-VIM) linear copolymer was firstly synthesized as follows: 1.5 g of NIPAM, 0.18 mL of VIM, and 0.036 g of AIBN were dissolved in 18 mL of DOA. The mixture was magnetically stirred and dissolved, and reacted at 70 °C for 24 h in a nitrogen atmosphere. After the reaction, the polymer solution was placed in a dialysis tube (molecular weight cut-off 8000–14000) and purified in water for 24 h, changing the water every 8 h. The purified P(NIPAM-*co*-VIM) linear copolymer was dried in a vacuum oven at 60 °C. The dried linear copolymer was dissolved in 60 mL of deionized water, and 118 μL of 1,5-dibromopentane was added as a crosslinking agent. The mixture obtained above was purged with nitrogen gas and reacted at 70 °C for 24 h. After the end of the reaction, the microgel dispersion was placed in a dialysis tube (molecular weight 8000–14000) and purified in deionized water for 24 h, changing the water every 8 h. By keeping the amount of NIPAM monomer constant, the mass fraction of VIM was controlled to be 11 wt%, 30 wt%, 50 wt%, and 70 wt%, which correspond to molar feed ratios of NIPAM/VIM of 1/0.14, 1/0.38, 1/0.63, and 1/0.89, respectively. Therefore, the synthesis of microgels with different mass fractions of VIM was achieved. Note that the amount of the crosslinker was kept constant for the synthesis of P(NIPAM-*co*-VIM) microgels. The PNIPAM microgel was prepared *via* the free radical polymerization of NIPAM. 0.891 g of NIPAM and 0.18 g of MBA crosslinker were dissolved in 45 mL of water, and the mixture was bubbled with nitrogen, stirred, and heated at 70 °C. Then, the initiator potassium

persulfate was added, and the reaction was allowed to carry on for 24 h. The purification and separation of PNIPAM microgels were similar to P(NIPAM-*co*-VIM) microgels.

2.3 Drawing of phosphate adsorption standard curve

1.0, 2.0, 3.0, 4.0, 5.0, 6.0, 7.0, and 8.0 mL of phosphate anion standard solutions with a concentration of 0.02 mg mL^{-1} were taken in 8 volumetric flasks with a volume of 50 mL, and each solution was diluted with about 25 mL water. Then, 5.0 mL of ammonium molybdate solution and 3.0 mL of ascorbic acid solution were added to each solution in the volumetric flask and diluted with water to the full scale of 50 mL. Fig. S1† shows pictures of blank solution and phosphomolybdate blue solutions prepared from eight groups of phosphate solutions with different concentrations (see ESI†). These groups of solutions were kept at room temperature for 10 min, and the spectrophotometric determination of phosphate was then performed at 890 nm using a UV-1800 ultraviolet spectrophotometer (Shimadzu, Japan). All measurements were made using cuvettes. The standard work curve was established, as shown in Fig. S2,† after having carried out the procedure of the standard work curve. The linear equation was obtained and the linear scope of phosphate concentration was 0.4–3.2 mg L^{-1}. The linear correlation coefficient R was 0.98, which means that this linear equation shows good linear correlation and can satisfy the photometric measurement of phosphate.

2.4 Phosphate anion adsorption experiment

Firstly, phosphate solutions with various concentrations of 0.05, 0.2, and 0.3 mg mL^{-1} were prepared in a 250 mL beaker, respectively. 0.05 g of dried microgel powder was dispersed in 10 mL of water, and then placed in a dialysis tube for adsorption. The whole solution was sealed with plastic wrap, and stirred magnetically at a certain temperature; the adsorption time was two days. The pre-adsorption and post-adsorption phosphate ion solutions were diluted to the concentration range of the standard curve, and their absorbance values were determined by the phosphorus–molybdenum blue method. The adsorption capacity is calculated as follows:

$$Q_e = \frac{C_0 V_0 - C_1 V_1}{m} \quad (1)$$

where Q_e is the adsorption capacity of the microgel for phosphate ions (mg g^{-1}), m is the mass of the dried microgel for adsorption (g), C_0 is the concentration of phosphate solution before adsorption (mg mL^{-1}), C_1 is the concentration of phosphate solution after adsorption (mg mL^{-1}), V_0 is the volume of phosphate solution before adsorption (mL), and V_1 is the sum of the volume of phosphate solution and the volume of the microgel solution (mL).

2.5 Influence of time on adsorption

0.2 g of $Na_3PO_4 \cdot 12H_2O$ was dissolved in 250 mL of water to obtain a phosphate solution with a low concentration of 0.2 mg mL^{-1}. The adsorption of phosphate anions by microgels was carried out, and the UV-vis absorbance values of the phosphate solution at regular time intervals were measured before and after adsorption. The influence of time on the phosphate adsorption of PNIPAM and P(NIPAM-*co*-VIM) microgels was investigated.

2.6 Influence of phosphate concentration on adsorption

0.05 g, 0.2 g, and 0.30 g of $Na_3PO_4 \cdot 12H_2O$ were dissolved in 250 mL of water, respectively. Phosphate solutions with different concentrations were obtained. The effect of phosphate concentration on phosphate adsorption by PNIPAM and P(NIPAM-*co*-VIM) microgels was studied.

2.7 Influence of pH on adsorption

0.2 g of $Na_3PO_4 \cdot 12H_2O$ was dissolved in 250 mL of water to obtain a phosphate solution, and the pH of the phosphate solution was adjusted to 5, 7, and 10, respectively. The influence of pH on phosphate adsorption of PNIPAM and P(NIPAM-*co*-VIM) microgels was studied.

2.8 Influence of temperature on adsorption

0.2 g of $Na_3PO_4 \cdot 12H_2O$ was dissolved in 250 mL of water to obtain a phosphate solution with a concentration of 0.2 mg g^{-1}. The temperature of the adsorption experiment was adjusted to 20 °C and 55 °C, respectively. The effect of temperature on the adsorption performance of the PNIPAM and P(NIPAM-*co*-VIM) microgels was investigated.

2.9 LbL self-assembly of polyelectrolyte/microgels on QCM sensor

Firstly, the QCM sensor (gold-coated AT-cut quartz crystal, fundamental frequency f_0 of 5 MHz, Suzhou Siju Biomaterials Co., Ltd., Suzhou, China) was cleaned with a mixture of deionized water, hydrogen peroxide, and ammonia with a volume ratio of 5 : 1 : 1. After cleaning, the QCM sensor was taken out and soaked in an ethanol solution, and then dried with nitrogen. The concentrations of PEI solution, PSS solution, and P(NIPAM-*co*-VIM) solution were 0.02 g mL^{-1}, 0.01 g mL^{-1}, and 0.048 mg mL^{-1}, respectively. The QCM sensor was placed in the flow cell of the QCM (iQCM equipment, Model QCM-A DBY-17, Hangzhou Longqin Advanced Materials Sci. & Tech. Co., Ltd., Hangzhou, China), and deionized water was passed into the QCM flow cell at a flow rate of 100 μL min^{-1}. The normalized frequency shift ($\Delta f_3/3$) of the QCM sensor was recorded at the third overtone ($n = 3$) as the baseline in deionized water. After stabilization, the PEI solution was first introduced. Due to the interaction between the amino groups of PEI and gold, the PEI chains were adsorbed onto the QCM sensor surface, leading to a decreased frequency shift of the QCM sensor. After the adsorption had reached equilibrium, the PSS solution was introduced and adsorption of the negatively charged PSS chains took place on the PEI layer. Finally, the positively charged microgel was introduced to form the self-assembled PEI/PSS/P(NIPAM-*co*-VIM) on the QCM sensor surface. The entire self-assembly process was monitored using the QCM.

2.10 Instruments and characterization

A scanning electron microscope (JSM-6360LA, JEOL, Japan) was used to observe the size and morphology of the samples. The microgel solution was dropped onto a glass sheet of 1 cm × 1 cm, and dried naturally at room temperature. The surface of the resulting sample was coated with a thin gold film before observation.

A Fourier transform infrared spectrometer (FT-IR, Thermo Nicolet Avatar 370, USA) was employed to characterize the samples. The prepared P(NIPAM-*co*-VIM) microgel was dried at 60 °C in a vacuum oven and dried into a white powder form. The powder of the microgel was mixed with KBr powder in a ratio of 1 : 100 to form tablets, and the FT-IR spectra of the PNIPAM and P(NIPAM-*co*-VIM) microgels were determined.

A zeta potentiometric and particle size analyzer (Zetasizer Nano ZS, Malvern) was adopted to analyze the zeta potential and particle size of the PNIPAM and P(NIPAM-*co*-VIM) microgels in aqueous solution. The pH of the solution was adjusted by HCl or NaOH. The temperature of the solution was set from 20 °C to 55 °C.

Tapping mode atomic force microscopy (AFM, NanoMan VS, Veeco Instrument Inc., USA) was adopted to determine the morphology of the QCM sensor surface before and after the self-assembly of the PEI/PSS/microgel at room temperature in air.

A contact angle measurement instrument (HARKE-SPCA, Beijing Harke Test Instrument, Beijing, China) was employed to test the water contact angle of the samples. The PNIPMAM and P(NIPAM-*co*-VIM) microgels were coated on a slide, and placed in a vacuum oven at 60 °C for drying. The contact angle between the microgel film and water was measured after drying to study its hydrophilicity.

The adsorption response of the self-assembled PEI/PSS/microgels to phosphate ions was studied using QCM. The self-assembled microgel-modified QCM sensors were fixed into the flow unit of the QCM, and deionized water was first passed at a flow rate of 100 μL min^{-1}. Taking the resonance frequency of the QCM sensor in deionized water as a reference, different concentrations of 10^{-8}, 10^{-7}, and 10^{-6} M of phosphate ion solutions were channeled into the flow unit. Because the self-assembled microgels contain many binding sites that can interact with phosphate ions, phosphate ions were adsorbed onto the surface of the self-assembled multilayer, leading to a decrease in the resonance frequency ($\Delta f_3/3$) of the QCM sensor. The mass per unit area of adsorbed phosphate ions can be calculated semi-quantitatively with the Sauerbrey[49] equation, which can be converted into number per unit area with the molar molecular weight of phosphate anions.

$$\Delta m = \frac{-C\Delta f_n}{n} \quad (2)$$

where the constant C is 17.7 ng cm^{-2} Hz^{-1}, n is the overtone, and Δf_n is the frequency change. The normalized QCM frequency change ($\Delta f_3/3$) was obtained at the third (n = 3, 15 MHz) harmonic. Similarly, during the self-assembly process, the mass of the adsorbed polyelectrolyte and microgel can also be calculated semi-quantitatively using this formula.

3 Results and discussion

3.1 Synthesis and formation mechanism of ionic microgels

A schematic reaction of the P(NIPAM-*co*-VIM) microgel is shown in Fig. 1. As shown in Fig. 1a, this work takes *N*-isopropyl acrylamide (NIPAM) as the main monomer and 1-vinyl imidazole (VIM) as a functional comonomer, and P(NIPAM-*co*-VIM) linear copolymer is firstly obtained by free radical copolymerization. Information including molecular weights and composition for the linear copolymer precursors of P(NIPAM-*co*-VIM) for synthesizing the microgels are of significance and should be characterized, in order to better understand the adsorption properties of the resulting microgels. Therefore, the NMR and GPC characterizations of the linear copolymer precursors of P(NIPAM-*co*-VIM) with different VIM fractions of 11%, 30%, 50%, and 70% were carried out, and their real ratios of NIPAM/VIM were calculated by NMR, and molecular weight and PDI by GPC are listed in Table S1 in the ESI.† From Table S1,† it can be seen that when the molar feed ratios of NIPAM/VIM were 1/0.14, 1/0.38, 1/0.63, and 1/0.89, the real ratios of NIPAM/VIM in copolymers by NMR were calculated to be 1/0.12, 1/0.33, 1/0.55, and 1/0.82, respectively. The molecular weights of P(NIPAM-*co*-VIM) with different VIM fractions of 11%, 30%, 50%, and 70% were found to be in the range from 4.92×10^4 to 6.14×10^4 with PDI values from 2.23 to 1.99. As shown in Fig. 1b and c, an aqueous solution of the linear copolymer is translucent at 15 °C, and the solution becomes milky white after heating at 45 °C; that is, when the temperature is increased to the LCST of the copolymer, the conformation shrinks and collapses due to a volume phase change, forming hydrophobic globules and a color change from clear to turbid. This demonstrated that a P(NIPAM-*co*-VIM) linear copolymer had been prepared. Finally (as shown in Fig. 1d), P(NIPAM-*co*-VIM) microgels were obtained by quaternary crosslinking between 1,5-dibromopentane (as the crosslinking agent) and the comonomer tertiary amine group. Note that the PNIPAM microgel could not be synthesized in the same way as the P(NIPAM-*co*-VIM) microgel. The NIPAM monomer has only a double bond in its molecular structure, and the linear NIPAM homopolymer chain can be synthesized *via* free radical polymerization initiated by AIBN. Since it is not like the P(NIPAM-*co*-VIM) copolymer and there is no VIM monomer unit, and it is impossible to form a PNIPAM microgel by crosslinking with 1,5-dibromopentane. Therefore, in this work, PNIPAM was prepared into a homopolymer microgel using MBA as a crosslinking agent. In order to illustrate the role of VIM monomer in P(NIPAM-*co*-VIM) microgels, the copolymer chains can be crosslinked by 1,5-dibromopentane during the preparation process and can be charged, and it is also easy to bind phosphate ions. In comparison, PNIPAM microgel is a completely homopolymeric microgel without VIM units or positively charged groups, and shows weak adsorption capacity for phosphate ions.

3.2 FT-IR, particle size, and SEM studies

Fig. 2 shows the FT-IR spectra of PNIPAM and P(NIPAM-*co*-VIM) microgels, the particle size of PNIPAM and P(NIPAM-*co*-VIM)

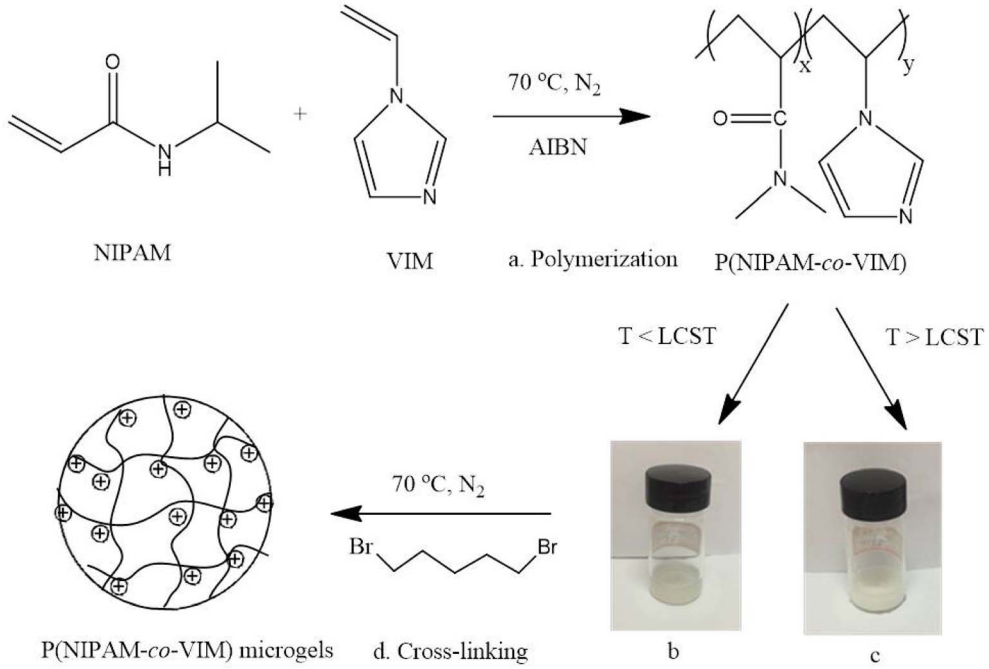

Fig. 1 Schematic of the synthesis of ionic P(NIPAM-*co*-VIM) microgels, including polymerization (a), linear P(NIPAM-*co*-VIM) copolymer solution at 20 °C (b) and 45 °C (c), and final crosslinking (d).

microgels as a function of temperature, and SEM photographs of PNIPAM and P(NIPAM-*co*-VIM) microgels. As shown in Fig. 2a, from the PNIPAM spectrum, the characteristic absorption peaks at 1642 cm^{-1} and 1546 cm^{-1} are attributed to the C=O and N–H stretching vibrations (amide characteristic absorption) of the NIPAM part, respectively. From the spectrum

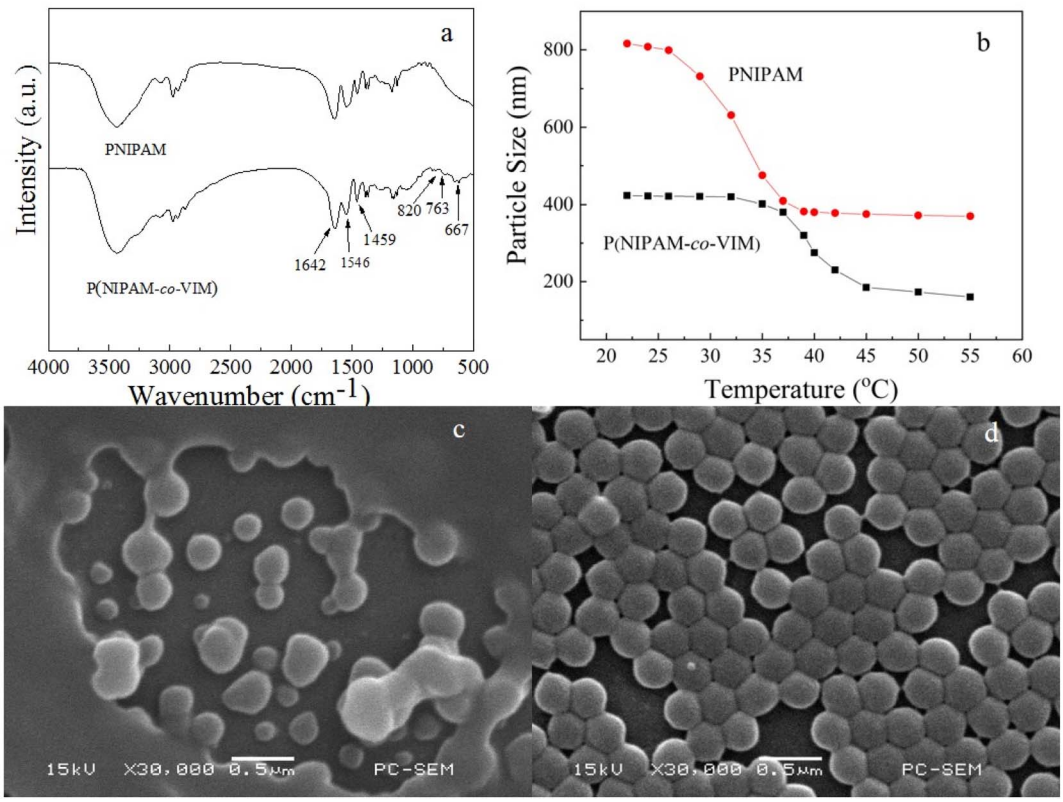

Fig. 2 FT-IR spectra of the PNIPAM and P(NIPAM-*co*-VIM) microgels (a), the particle size of the PNIPAM and P(NIPAM-*co*-VIM) microgels as a function of temperature (b), and SEM images of the PNIPAM (c) and P(NIPAM-*co*-VIM) microgels (d).

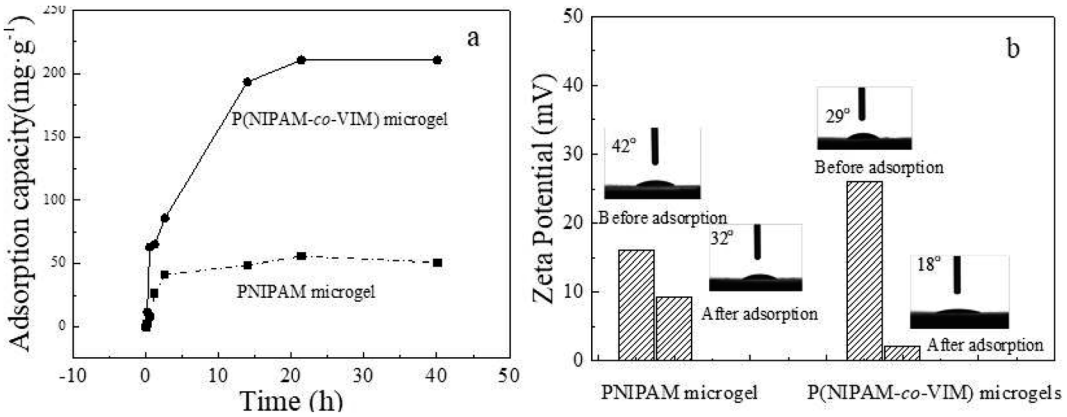

Fig. 3 The curve of the adsorption capacity of PNIPAM and P(NIPAM-*co*-VIM) microgels for phosphate ions over time (a). Zeta potentials and water contact angles of PNIPAM and P(NIPAM-*co*-VIM) microgels before and after adsorption of phosphate ions (b).

of P(NIPAM-*co*-VIM), it can be seen that the peak at 3100 cm^{-1} belongs to the C–H stretching vibration of the imidazole ring,[50] and the absorption band at 1459 cm^{-1} belongs to the stretching vibrations of the C=C and C=N groups in the imidazole ring. In addition, the peaks at 820, 763, and 667 cm^{-1} are ascribed to the deformation out-of-plane-bending of the imidazole ring. Based on these results, the P(NIPAM-*co*-VIM) microgel was successfully synthesized by a two-step method. As can be seen from Fig. 2b, the particle size of both PNIPAM and P(NIPAM-*co*-VIM) microgels decreases as the temperature increases, due to the presence of NIPAM in the feedstock of the microgel, which is a temperature-sensitive monomer. When the temperature is

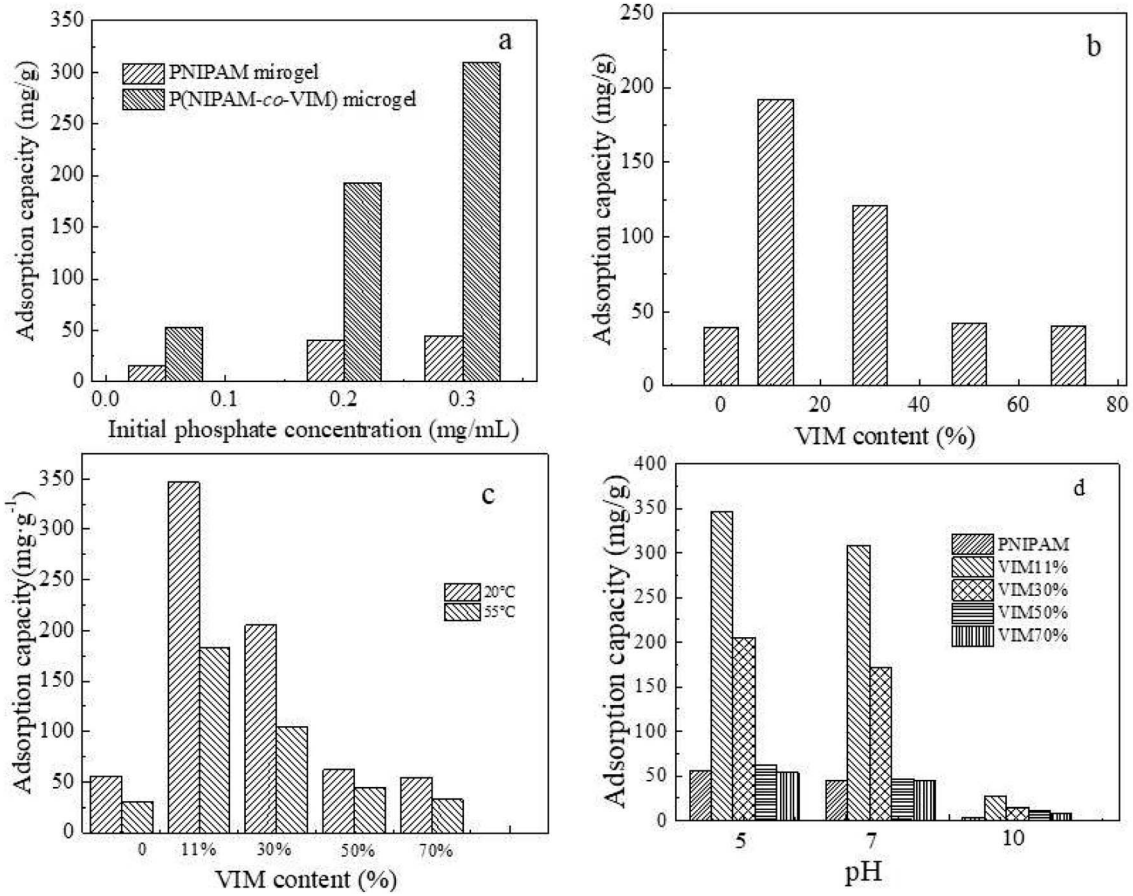

Fig. 4 The adsorption capacities of PNIPAM and P(NIPAM-*co*-VIM) microgels for phosphate ions at different phosphate solution concentrations (a), different VIM contents (b), temperature (c), and pH (d).

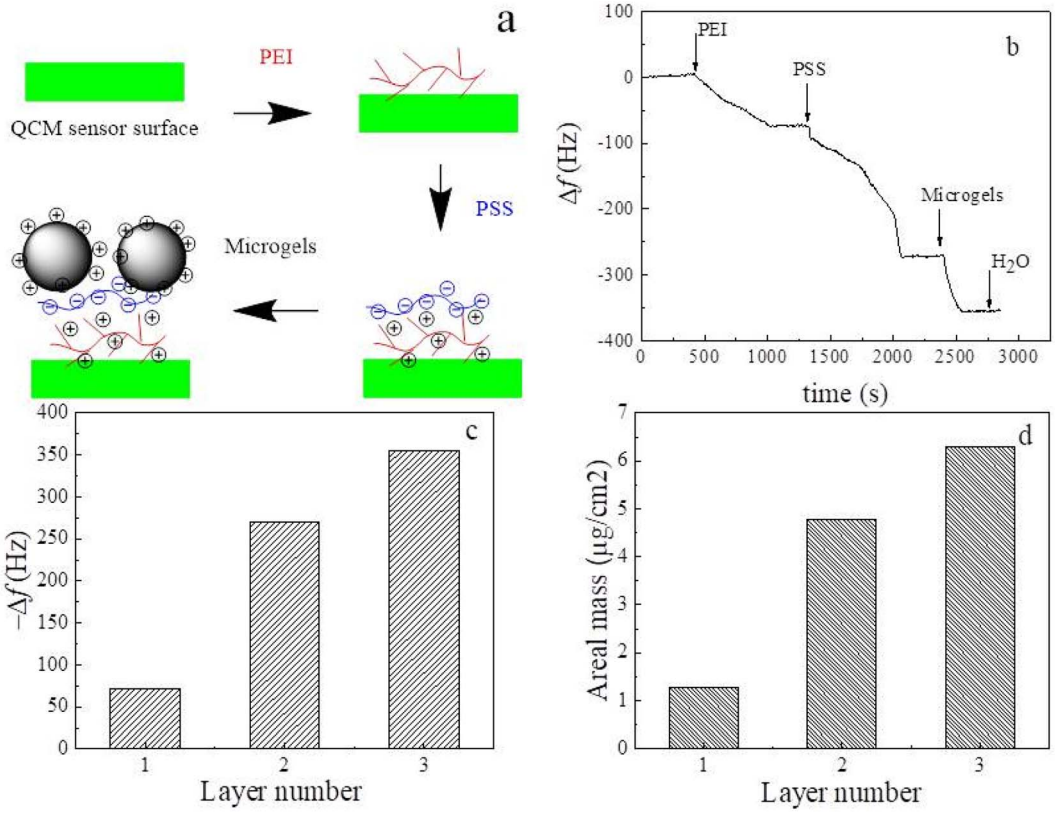

Fig. 5 Schematic diagram of the self-assembly process of PEI/PSS/(PNIPAM-*co*-VIM) microgels (a). The frequency shift of the microgel-modified QCM sensor over time during self-assembly (b). The frequency shift of the QCM sensor for the surface adsorption of PEI, PSS, and microgel at equilibrium as a function of layer number (c), and the corresponding areal mass for the surface adsorption of PEI, PSS, and microgel at adsorption equilibrium as a function of the layer number (d).

lower than the lower critical solution temperature (LCST, ~32 °C) of the temperature-sensitive PNIPAM chain,[51] it will be hydrophilic and have an expanded swollen structure; when the temperature is higher than its LCST, it will become hydrophobic, shrink, and become a compact globule. Fig. 2b shows the change in the particle size of PNIPAM and P(NIPAM-*co*-VIM) microgels with temperature. From Fig. 2b, at 26 °C, the particle size of the PNIPAM microgel is about 790 nm. With an increase in the test temperature, at 32 °C, the particle size dropped sharply; that is, 32 °C is the phase transition temperature of the PNIPAM microgel. Compared to the PNIPAM microgel, the P(NIPAM-*co*-VIM) microgel has a particle size of about 420 nm at 26 °C. This particle size difference between the PNIPAM microgel and the P(NIPAM-*co*-VIM) microgel is due to differences in synthesis method, composition, and crosslinking density. From Fig. 2b, it can be observed that its particle size decreases with an increase in temperature, and the phase transition temperature of the P(NIPAM-*co*-VIM) microgel is about 37.5 °C, attributed to the hydrophilicity of VIM and the electrostatic repulsion caused by partial ionization. From the SEM images in Fig. 2c and d for the PNIPAM and P(NIPAM-*co*-VIM) microgels, respectively, it can be seen that the synthesized temperature-sensitive microgels are all spherical particles. In Fig. 2c, the microgel particles at the edges are bonded together to form a thick film layer, and it can be seen from the middle part that the diameter of the particles is about 400–500 nm. In Fig. 2c, there are several larger particles at the edges, which may be due to the aggregates of small microgel particles during SEM sample preparation, including the microgel swelling and drying, while the P(NIPAM-*co*-VIM) microgel particles in Fig. 2d are more uniform, with a diameter of about 200–300 nm. It can be seen from the SEM results that the particle size of the ionic P(NIPAM-*co*-VIM) microgel prepared by the two-step method seems smaller than the particle size of the microgel measured by the particle size analyzer in solution.

3.3 Adsorption curve, zeta potential, and water contact angle tests

Fig. 3a shows the variation in the phosphate adsorption capacity of the PNIPAM and P(NIPAM-*co*-VIM) microgels over time (where the concentration of phosphate ions is 0.2 mg mL^{-1}, the adsorption temperature is 20 °C, and pH = 5). As can be seen from Fig. 3a, with an increase in time, the adsorption capacity of the microgels for phosphate ions increased, and the adsorption reached equilibrium at 30 h. In contrast, when the adsorption equilibrium was reached, the adsorption capacity of the PNIPAM microgel for phosphate ions reached 50.8 mg g^{-1}. The adsorption capacity of the P(NIPAM-*co*-VIM) microgel for phosphate ions reached 210.7 mg g^{-1}. The adsorption capacity

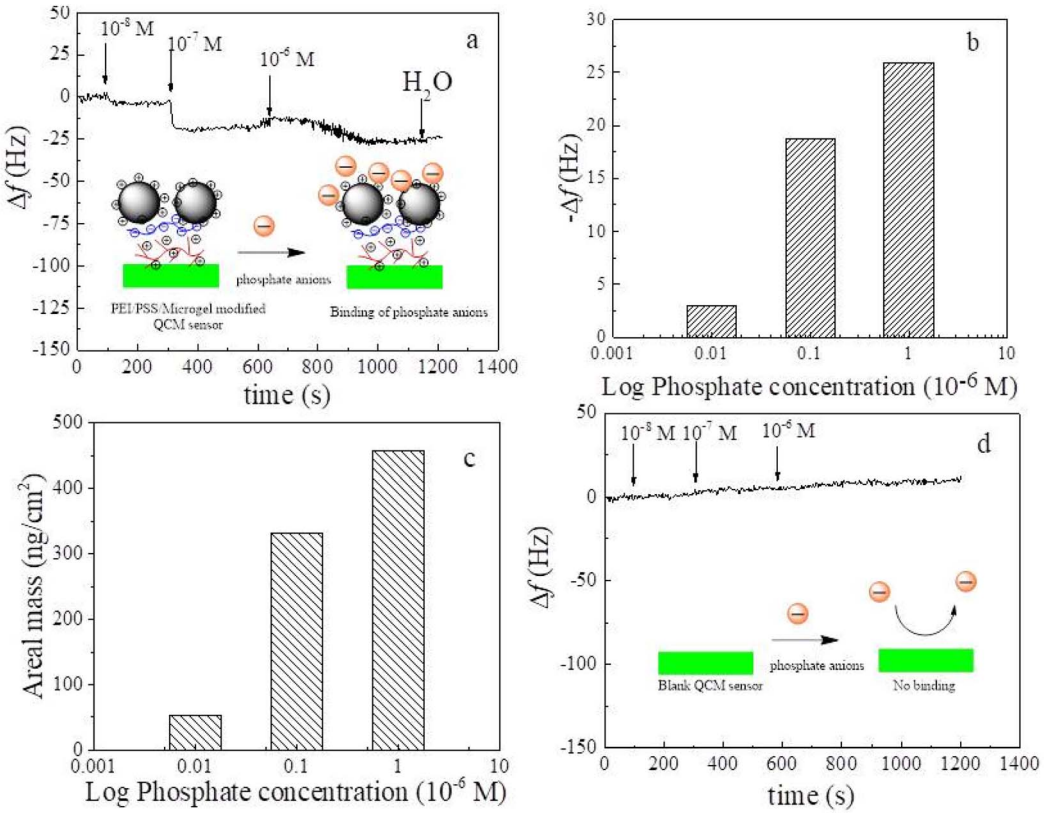

Fig. 6 Frequency response of PEI/PSS/(PNIPAM-*co*-VIM) microgel-modified QCM sensors to different concentrations of phosphate ions (10^{-8}, 10^{-7}, and 10^{-6} M) (a). The insert shows the adsorption mechanism of the self-assembled PEI/PSS/(PNIPAM-*co*-VIM) microgel for phosphate ions. The frequency response (b) and areal mass (c) of the microgel-modified QCM sensor at saturation as a function of phosphate concentration. Adsorption response of a blank QCM sensor to different phosphate ions and its interaction mechanism (d).

of the P(NIPAM-*co*-VIM) microgel for phosphate ions is better than that of the PNIPAM microgel for phosphate ions, which is due to the excellent anion adsorption capacity of the quaternized imidazole groups in the P(NIPAM-*co*-VIM) microgel, which can bind to phosphate ions by electrostatic force, and since the counter ions (Br^-) in the microgel can be replaced by

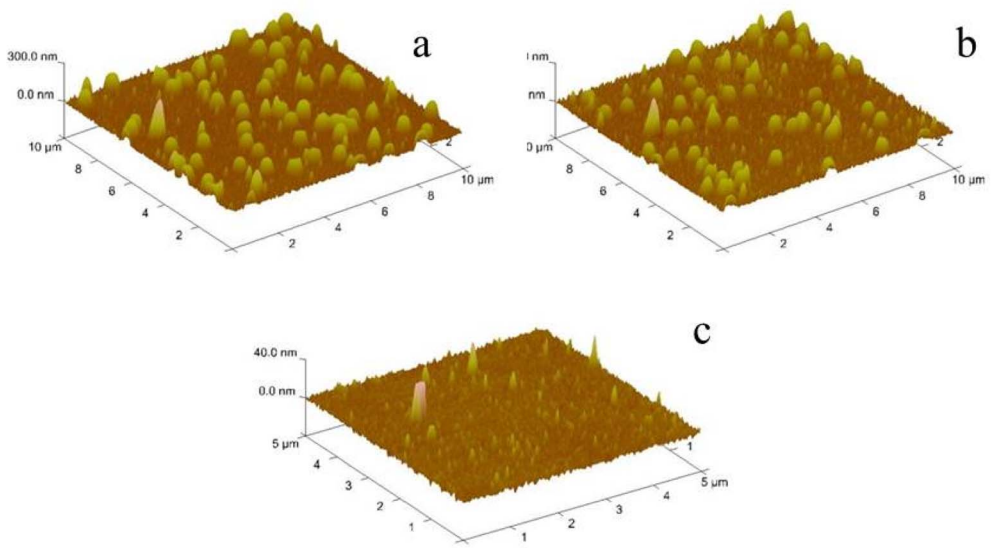

Fig. 7 Three-dimensional AFM topography height maps of the self-assembled PEI/PSS/(PNIPAM-*co*-VIM) microgel before (a) and after (b) the adsorption of phosphate ions on the QCM sensor surface, and blank QCM sensor (c).

Table 1 Comparison of phosphate ion adsorption properties of different adsorption materials

Adsorption materials	Cu^{2+} ions-loaded poly(AAc/AM/SH) hydrogels	Ferrihydrite	Graphene	P(NIPAM-*co*-VIM) microgel
Adsorption capacity (mg g^{-1})	87.62	104.8	89.37	346.3

phosphate ions by an ion exchange reaction. This makes the adsorption property of P(NIPAM-*co*-VIM) microgels for phosphate ions much better than that of the PNIPAM microgel. Fig. 3b shows the potential test results of the PNIPAM and P(NIPAM-*co*-VIM) microgels before and after the adsorption of phosphate ions. The initial zeta potentials of the P(NIPAM-*co*-VIM) and PNIPAM microgels are 26.1 mV and 16.0 mV, respectively, which are conducive to the adsorption of phosphate ions. After the adsorption of phosphate ions, the zeta potential values of the P(NIPAM-*co*-VIM) and PNIPAM microgels drop to 2.2 mV and 9.3 mV, respectively. This is due to the adsorption of negatively charged phosphate ions, and the potential drops naturally after the microgel binds to the phosphate ions. As can be seen from Fig. 3b, the potential difference of the P(NIPAM-*co*-VIM) microgel after adsorption of phosphate ions is greater than that of the PNIPAM microgel, indicating there are more phosphate ions bound to the P(NIPAM-*co*-VIM) microgels than those bound to PNIPAM microgel. Fig. 3b also shows the water contact angle between the PNIPAM and P(NIPAM-*co*-VIM) microgels and water. As can be seen from Fig. 3b, the water contact angle before the PNIPAM microgel adsorbs phosphate ions is 42°. After the adsorption of phosphate ions, the water contact angle is 32°. The P(NIPAM-*co*-VIM) microgel has a contact angle of 29° with water before the adsorption of phosphate ions, and 18° with water after the adsorption of phosphate ions. As can be seen from the results of the contact angle, both PNIPAM and P(NIPAM-*co*-VIM) microgels exhibit good hydrophilicity properties, due to the presence of hydrophilic amino groups in the microgels, which form hydrogen bonds with water. Moreover, the contact angle with water after the adsorption of phosphate ions is reduced, due to the binding of phosphate anions contained in the adsorption microgel, which are oxygenated anions, which can form hydrogen bonds with water molecules. In contrast, P(NIPAM-*co*-VIM) microgels are more hydrophilic due to the presence of quaternary imidazole groups within them, which bind well to water through hydrogen bonds. As a result, the hydrophilic performance of microgels with the addition of functional monomer VIM has improved. Zeta potentials and water contact angles for P(NIPAM-*co*-VIM) microgels containing different VIM contents were also measured. It can be seen that zeta potentials for P(NIPAM-*co*-VIM) microgels with different VIM mass fractions of 11%, 30%, 50%, and 70% were 26.1, 27.4, 28.2, and 29.1 mV, respectively. In addition, the water contact angles for P(NIPAM-*co*-VIM) microgels with different VIM mass fractions of 11%, 30%, 50%, and 70% were found to be 29°, 27°, 24°, and 21°, respectively. These results indicate the influence of the amount of VIM units with functionality of charged groups and hydrophilic nature on the properties of the formed P(NIPAM-*co*-VIM) microgels.

3.4 Influence of phosphate solution concentrations, VIM content, temperature, and pH

Fig. 4 shows the adsorption capacity of PNIPAM and P(NIPAM-*co*-VIM) microgels for phosphate ions at different phosphate solution concentrations, different VIM contents, temperature (Fig. 4c), and pH (Fig. 4d). As can be seen from Fig. 4a, the phosphate ion concentration does affect the adsorption capacity of the microgel (the adsorption temperature is 20 °C, pH = 7). When the concentration of phosphate ions in an aqueous solution was 0.05 mg mL^{-1}, the adsorption capacities of the PNIPAM and P(NIPAM-*co*-VIM) microgels for phosphate ions were 16.1 mg g^{-1} and 52.4 mg g^{-1}, respectively. When the concentration of phosphate ions in an aqueous solution was 0.20 mg mL^{-1}, the adsorption capacities of the PNIPAM and P(NIPAM-*co*-VIM) microgels for phosphate ions increased to 39.6 mg g^{-1} and 192.3 mg g^{-1}, respectively. When the concentration of phosphate ions in aqueous solution was 0.30 mg mL^{-1}, the adsorption capacities of the PNIPAM and P(NIPAM-*co*-VIM) microgels for phosphate ions were 44.5 mg g^{-1} and 309.0 mg g^{-1}, respectively. It can be seen that for low or high concentrations of phosphate ions, P(NIPAM-*co*-VIM) microgels all have a certain adsorption ability. Fig. 4b shows the adsorption amounts of phosphate ions in four groups of microgels with VIM contents of 0, 11%, 30%, 50%, and 70%, respectively (the concentration of phosphate ion solution is 0.2 mg mL^{-1}, the adsorption temperature is 20 °C, and pH = 7). As can be seen from Fig. 4b, the adsorption capacity for phosphate ions by a pure PNIPAM microgel is 39.6 mg g^{-1} under these conditions. After adding VIM with different mass fractions of 11 wt%, 30 wt%, 50 wt%, and 70 wt%, the adsorption capacities of P(NIPAM-*co*-VIM) microgels for phosphate ions were 192.3, 120.5, 42.1, and 40.4 mg g^{-1}, respectively, and their adsorption ability was better than that of microgels without VIM, due to electrostatic interactions, hydrogen bonding, and ion exchange between microgels and phosphate ions. When the VIM content is 11%, the adsorption capacity of the microgel for phosphate ions is significant, which also shows that the introduction of VIM does not follow the rule of the more the better, since too much VIM may affect the network structure of the P(NIPAM-*co*-VIM) microgel. When the VIM content gradually increases, the phase transition temperature of the obtained copolymer also moves in the direction of high temperature, and the phase transition is not easily observed, resulting in the morphology and size of the microgel becoming more and more uncontrollable at the same preparation temperature, and the internal crosslinking network structure of the microgel is also not perfect and regular, resulting in a decrease in the adsorption amount of phosphate anions achieved. A microgel with a normal and complete network structure also plays a crucial role in the adsorption of phosphate ions. Fig. 4c shows a histogram of the adsorption of phosphate ions by four groups

of microgels with VIM contents of 0, 11%, 30%, 50%, and 70%, respectively (where the concentration of phosphate ions is 0.3 mg mL^{-1}, the adsorption temperature is 20 °C, pH = 5). As can be seen from Fig. 4c, the adsorption capacities of pure PNIPAM microgels for phosphate ions at 20 °C and 55 °C are 55.6 and 30.3 mg g^{-1}, respectively. At 20 °C, after adding VIMs with different mass fractions of 11 wt%, 30 wt%, 50 wt%, and 70 wt%, the adsorption capacities of P(NIPAM-*co*-VIM) microgels for phosphate ions were 346.3, 205.3, 61.9, and 53.8 mg g^{-1}, respectively. Similarly, at 55 °C, after adding VIMs with different mass fractions of 11 wt%, 30 wt%, 50 wt%, and 70 wt%, the adsorption capacities of P(NIPAM-*co*-VIM) microgels for phosphate ions were 182.5, 105.1, 44.1, and 32.6 mg g^{-1}, respectively. At high temperatures, the adsorption of phosphate ions by ionic P(NIPAM-*co*-VIM) microgels decreases. According to a temperature sensitivity test of P(NIPAM-*co*-VIM) microgels, the particle size shows a sharp change with an increase in temperature. The volume phase transition temperature (VPTT) of a P(NIPAM-*co*-VIM) microgel in an aqueous solution occurs at about 37.5 °C. When the temperature is lower than VPTT, the microgel swells in water, resulting in a volume increase. When the temperature is higher than VPTT, the microgel undergoes a contraction in the water, resulting in a decrease in volume. Therefore, compared to the shrinking state at 55 °C, the P(NIPAM-*co*-VIM) microgel at 20 °C is swelling and has a large volume and an expanding network, allowing the binding of phosphate ions on the microgel. This also shows that temperature does have an effect on the adsorption of phosphate ions by P(NIPAM-*co*-VIM) microgels, and a larger adsorption capacity can be obtained when the temperature is lower than the VPTT. A study on the degree of swelling of the final microgels as a function of pH is helpful to gain a better understanding of the adsorption ability of the resulting microgels when the pH values varies. Fig. S3† shows the particle size of the final swollen P(NIPAM-*co*-VIM) microgels as a function of pH (see ESI, Fig. S3†). From Fig. S3,† it can be seen that the particle size and swelling of P(NIPAM-*co*-VIM) microgels were greatly influenced by pH. At a low pH (acidic solution), P(NIPAM-*co*-VIM) microgels containing VIM groups are easily positively charged on its network, leading to more binding sites and a high degree of swelling, which is beneficial for adsorbing more phosphate anions. In contrast, at a high pH (alkaline solution), the number of positively charged groups on the network of P(NIPAM-*co*-VIM) microgels containing VIM groups decreased, resulting in a reduced number of binding sites and a low degree of swelling, which is not helpful for interacting with phosphate anions. Fig. 4d displays the change of the adsorption capacities of four groups of microgels with VIM contents of 0, 11%, 30%, 50%, and 70% respectively (wherein the phosphate ion concentration was 0.30 mg mL^{-1} and the adsorption temperature was 20 °C). Under the condition of neutral pH = 7, the adsorption capacities of pure PNIPAM microgel and P(NIPAM-*co*-VIM) microgels with different mass fractions of 11%, 50%, and 70% were 44.5, 309.0, 172.1, 46.8, and 44.3 mg g^{-1}, respectively. Under alkaline conditions, the adsorption capacities of phosphate ions by pure PNIPAM microgel and P(NIPAM-*co*-VIM) microgels with different mass fractions of 11%, 30%, 50%, and 70% were 4.1, 26.7, 14.9, 10.5, and 8.3 mg g^{-1}, respectively. As can be seen from Fig. 4d, the adsorption capacity of the microgel for phosphate decreases with an increase in pH from 5 to 10. When the solution is acidic, the adsorption capacity of the microgel for phosphate is the largest; when the solution is alkaline, the adsorption capacity is reduced. This is because the presence of H^+ at pH = 5 causes the potential values of the solution and microgel to rise, and the adsorption capacity of the microgel for phosphate ions increases due to electrostatic attraction. When pH = 10, the presence of OH^- makes the solution and microgel negatively charged, and since OH^- and phosphate ions are negatively charged ions and there is repulsion, the adsorption amount is reduced.

3.5 Self-assembly process of ionic microgels and polyelectrolyte on QCM sensors

Fig. 5 shows a schematic diagram of the self-assembly process of the PEI/PSS/(PNIPAM-*co*-VIM) microgel on the QCM sensor surface, the frequency changes of the modified QCM sensor with time during the self-assembly process, the frequency shift and surface adsorption areal mass of the modified QCM sensor when the surface adsorption of PEI, PSS, and microgel reaches equilibrium with the number of layers. The zeta potential of the P(NIPAM-*co*-VIM) microgel can reach 26.1 mV with a positive charge on the surface. Using the charged characteristics of ionic microgels, the self-assembled multilayer film is constructed on the surface of the QCM sensor, and is used as the sensing coating. The high sensitivity of the QCM sensor that can detect mass changes in the ng range is used for the detection of trace phosphate ions in water. From Fig. 5a, a layer of PEI polymer is first adsorbed on the gold surface of the QCM sensor using the strong interaction of the amino group of PEI with gold. Subsequently, a negatively charged PSS chain is introduced and adsorbed on the surface of the positively charged PEI layer by electrostatic attraction. Finally, by electrostatic interaction, a layer of positively charged P(NIPAM-*co*-VIM) microgel is adsorbed on the top of the PSS layer. Fig. 5b shows the curve of the frequency shift of the P(NIPAM-*co*-VIM) microgel-modified QCM sensor over time during the self-assembly process. As can be seen from Fig. 5b, the frequency shift of the blank QCM sensor is first stabilized in deionized water and serves as a baseline. As the PEI solution is introduced into the flow unit of QCM, the PEI molecular chain gradually adsorbs to the surface of the QCM sensor due to the interaction between amino and gold, and the frequency shift of the QCM sensor decreases significantly. Subsequently, the negatively charged PSS and the positively charged P(NIPAM-*co*-VIM) microgel were introduced, and the phenomenon of electrostatic adsorption behavior and frequency decrease was also found. As can be seen from Fig. 5c and d, the frequency shifts corresponding to the adsorption saturation of each layer of PEI, PSS, and microgel alone are 71.7, 198.5, and 85.1 Hz, and the areal masses of the adsorption calculated with the Sauerbrey equation are 1.27, 3.51, and 1.49 μg cm^{-2}, respectively. The areal mass value of the microgel adsorbed on the QCM sensor is close to the value of 4.876 μg cm^{-2} with microgels reported by Cao *et al.*[24] Cao *et al.* prepared

anionic poly(*N*-isopropyl acrylamide-*co*-acrylic acid) [P(NIPAM-*co*-AA)] microgels, and studied the self-assembly behavior of these anionic microgels and their response to heavy metal ions in water using QCM technology.

3.6 Interaction of the self-assembled microgels with phosphate anions by QCM

QCM sensors can detect the mass of adsorbent substances in the nanogram range of quartz crystal surfaces. With this property, it can be used to detect trace amounts of phosphate ions in ambient waters. Fig. 6 shows the frequency response of a blank QCM sensor modified with PEI/PSS/(PNIPAM-*co*-VIM) microgel to different concentrations of phosphate ions (10^{-8}, 10^{-7}, 10^{-6} M). The insert shows the adsorption mechanism of the self-assembled PEI/PSS/(PNIPAM-*co*-VIM) microgel on phosphate ions. Phosphate ions can be adsorbed on the surface of the QCM sensor by electrostatic attraction of positively charged groups on the microgel network structure. As can be seen from Fig. 6a, the frequency shift of the QCM sensor modified with the self-assembled PEI/PSS/(PNIPAM-*co*-VIM) microgel is stabilized in deionized water and can be used as the baseline. Subsequently, a phosphate anion solution of 10^{-8} mol L^{-1} was introduced into the flow unit of the QCM, and it can be seen from Fig. 6a that the frequency shift of the modified QCM sensor gradually decreased to −3.0 Hz, and the final adsorption equilibrium was reached, indicating that the self-assembled microgel modified QCM sensor had an adsorption response to 10^{-8} mol L^{-1} phosphate solution. When phosphate anion solutions with higher concentrations of 10^{-7} mol L^{-1} and 10^{-6} mol L^{-1} were introduced, the frequency shift of the modified QCM sensor continued to decrease. Fig. 6b shows the logarithmic plot of the frequency response of the microgel-modified QCM sensor and phosphate ion solution concentration when the adsorption microgels for phosphate anions reach equilibrium at each phosphate solution concentration. From Fig. 6b, the frequency responses corresponding to concentrations of 10^{-8}, 10^{-7}, and 10^{-6} M phosphate ions are 3.0, 18.8, and 25.9 Hz, respectively. If the areal mass of the adsorbed phosphate ions is approximated using the Sauerbrey equation, as shown in Fig. 6c, the areal masses corresponding to concentrations of 10^{-8}, 10^{-7}, and 10^{-6} M phosphate ions are 53.6, 332.0, and 458.2 ng cm^{-2}. As can be seen from Fig. 6d, there is no adsorption response to phosphate ions at concentrations of 10^{-8}, 10^{-7}, and 10^{-6} M due to the absence of functional microgel modification on the surface of the blank QCM sensor. The mechanism of interaction is shown in the insert to Fig. 6d. It can be seen that with ionized microgels as a sensing coating for QCM, QCM technology can be used to detect trace amounts of phosphate ions in the environment.

3.7 Morphology analysis

Fig. 7 shows three-dimensional AFM topography height maps of the self-assembled PEI/PSS/(PNIPAM-*co*-VIM) microgel before (Fig. 7a) and after (Fig. 7b) the adsorption of phosphate ions on the surface of the QCM sensor. To illustrate, this figure shows a morphology of the sample obtained in a dry state of air, which is different from the morphology of the swelling state dispersed in solution. As can be seen from Fig. 7a and b, the charged P(NIPAM-*co*-VIM) microgel successfully self-assembles with the polyelectrolyte on the gold electrode surface of the QCM sensor, with a spherical distribution, the surface is not fully covered, and the particle size of the microgel is around 300 nm. After the adsorption of phosphate ions, it remains spherical in a distributed state, and the self-assembled microgel remains stable on the QCM sensor surface without shedding. AFM images of the blank QCM sensor surfaces show that no microgel particles are found and the surface has a low roughness and is relatively smooth.

3.8 Comparison of adsorption properties of different materials

Table 1 shows a comparison of the phosphate anion adsorption properties of different adsorption materials. The maximum adsorption capacity of the P(NIPAM-*co*-VIM) microgel prepared in this study for phosphate ions is 346.3 mg g^{-1}. Singh *et al.*[52] prepared a copper-ion-supported poly(acrylic acid/acrylamide/sodium humate) poly(AAc/AM/SH) hydrogel for the adsorption of phosphate anions, and its adsorption capacity for phosphate ions was 87.62 mg g^{-1}. The study found that electrostatic interaction, ion pairing, and Lewis acid–base interaction work together to enhance the adsorption of phosphate ions. Mallet *et al.*[53] studied the adsorption of phosphate ions on ferrihydrite with a maximum adsorption capacity of 104.8 mg g^{-1}, which is mainly attributed to the formation of chemical bonds between Fe and phosphate ions on the surface of ferrihydrite. Vasudevan *et al.*[54] reported that graphene has an adsorption capacity of phosphate ions up to 89.37 mg g^{-1}. It can be seen that the adsorption property of the P(NIPAM-*co*-VIM) microgel prepared in this study is better than that of the other three materials, but further efforts are still needed to prepare materials with an efficient adsorption effect on phosphorus or phosphate ions.

4 Conclusions

This study showed that the addition of functional monomer VIM improved the adsorption of phosphate ions by microgels. The synthetic microgel has temperature sensitivity and good hydrophilicity, temperature exerts a certain influence on its adsorption of phosphate ions, and the adsorption property is better when the temperature is lower than the VPTT. The adsorption results showed that the adsorption property of P(NIPAM-*co*-VIM) microgel on phosphate ions was much better than that of PNIPAM microgel, due to the positive electric charge of the P(NIPAM-*co*-VIM) microgel and because it contains a quaternized imidazole ring, which could form strong binding with phosphate ions. When the mass fraction of VIM is 11%, pH = 5, and the temperature is 20 °C, P(NIPAM-*co*-VIM) has the largest adsorption capacity for phosphate ions, and the adsorption capacity can reach 346.3 mg g^{-1}. The layer-by-layer self-assembly results of the microgel with polyelectrolyte show that the P(NIPAM-*co*-VIM) microgel can be self-assembled on the QCM sensor surface, and its self-assembly multilayer has

a certain adsorption response to phosphate ions. Compared with the adsorption performance of several other materials, the ionic P(NIPAM-*co*-VIM) microgel prepared in this work has certain advantages in the adsorption of phosphate ions, and is expected to be used in the field of phosphate ion adsorption and sensing.

Author contributions

Jianping Yang: experiments, methodology, overall, investigation, and writing original draft. Bei Huang: experiments, data analysis, proofreading, and editing. Zhengxiang Lv: revision and editing. Zheng Cao: conceptualization, supervision, resources, funding acquisition, revision, and editing.

Conflicts of interest

The authors declare no conflicts of interest.

Acknowledgements

This project is supported by the National Natural Science Foundation of China (Grant No. 21704008), Major Science and Technology Project of Changzhou Health Commission (Project No: ZD201917), Natural Science Foundation of Jiangsu Province, China (Grant No. BK20201449), Natural Science Foundation of the Jiangsu Higher Institutions of China (Grant No. 20KJA430011). Financial support provided for this project by the Priority Academic Program Development of Jiangsu Higher Education Institutions (PAPD) and the Top-notch Academic Programs Project of Jiangsu Higher Education Institutions (TAPP), and financial support from the Young Elite Scientist Sponsorship Program of the Jiangsu Province Association of Science and Technology, Postgraduate Research & Practice Innovation Program of Jiangsu Province are also gratefully acknowledged.

References

1 Z. Cao, B. Du, T. Chen, J. Nie, J. Xu and Z. Fan, *Langmuir*, 2008, **24**, 12771–12778.
2 R. H. Pelton and P. Chibante, *Colloids Surf., A*, 1986, **20**, 247–256.
3 L. S. Benee, M. J. Snowden and B. Z. Chowdhry, *Langmuir*, 2002, **18**, 6025–6030.
4 B. R. Saunders, *Langmuir*, 2004, **20**, 3925–3932.
5 M. Bradley and B. Vincent, *Langmuir*, 2005, **21**, 8630–8634.
6 I. Berndt and W. Richtering, *Macromolecules*, 2003, **36**, 8780–8785.
7 D. Gan and L. A. Lyon, *J. Am. Chem. Soc.*, 2001, **123**, 7511–7517.
8 Z. Cao, Y. Chen, C. Zhang, J. Cheng, D. Wu, W. Ma, C. Liu and Z. Fu, *Soft Matter*, 2019, **15**, 2950–2959.
9 G. Liu, C. Liu, Y. Chen, S. Qin, S. Yang, D. Wu, H. Xi and Z. Cao, *Nanosci. Nanotechnol.–Asia*, 2019, **9**, 267–277.
10 Z. Cao, Y. Hu, Q. Yu, Y. Lu, D. Wu, A. Zhou, W. Ma, Y. Xia, C. Liu and K. Loos, *Adv. Eng. Mater.*, 2017, **19**, 1600826.
11 Z. Cao, T.-y. Chen, X.-l. Guo, X.-j. Zhou, J.-j. Nie, J.-t. Xu, Z.-q. Fan and B.-y. Du, *Chin. J. Polym. Sci.*, 2011, **29**, 439–449.
12 H. J. M. Wolff, M. Kather, H. Breisig, W. Richtering, A. Pich and M. Wessling, *ACS Appl. Mater. Interfaces*, 2018, **10**, 24799–24806.
13 R. Schroeder, W. Richtering, I. I. Potemkin and A. Pich, *Macromolecules*, 2018, **51**, 6707–6716.
14 M. Zhu, D. Lu, S. Wu, Q. Lian, W. Wang, A. H. Milani, Z. Cui, N. T. Nguyen, M. Chen, L. A. Lyon, D. J. Adlam, A. J. Freemont, J. A. Hoyland and B. R. Saunders, *ACS Macro Lett.*, 2017, **6**, 1245–1250.
15 M. Lehmann, W. Tabaka, T. Möller, A. Oppermann, D. Wöll, D. Volodkin, S. Wellert and R. v. Klitzing, *Langmuir*, 2018, **34**, 3597–3603.
16 H. Dong, V. Mantha and K. Matyjaszewski, *Chem. Mater.*, 2009, **21**, 3965–3972.
17 Y. Zhang, Z. Cao, Z. Luo, W. Li, T. Fu, W. Qiu, Z. Lai, J. Cheng, H. Yang, W. Ma and C. Liu, *J. Polym. Sci.*, 2022, **60**, 2329–2342.
18 J. Yang, K. Wang, Z. Lv, W. Li, K. Luo and Z. Cao, *ACS Omega*, 2021, **6**, 28285–28296.
19 Z. Cao, Y. Zhang, K. Luo, Y. Wu, H. Gao, J. Cheng, C. Liu, G. Tao, Q. Guan and L. Zhang, *J. Renewable Mater.*, 2021, **9**, 1447–1462.
20 Y. Wu, Y. Zhang, K. Wang, Z. Luo, Z. Xue, H. Gao, Z. Cao, J. Cheng, C. Liu and L. Zhang, *ACS Omega*, 2021, **6**, 5764–5774.
21 C. Zhang, Y. Dai, Y. Wu, G. Lu, Z. Cao, J. Cheng, K. Wang, H. Yang, Y. Xia, X. Wen, W. Ma, C. Liu and Z. Wang, *Carbohydr. Polym.*, 2020, **234**, 115882.
22 F. Zhao, X. Qin and S. Feng, *RSC Adv.*, 2016, **6**, 100511–100518.
23 B. Wen, J. Xue, X. Zhou, Q. Wu, J. Nie, J. Xu and B. Du, *ACS Appl. Mater. Interfaces*, 2018, **10**, 25706–25716.
24 Z. Cao, Y. Chen, Q. Zhang, Y. Xia, G. Liu, D. Wu, W. Ma, J. Cheng and C. Liu, *Nanofabrication*, 2017, **3**, 16–25.
25 S. Hamoudi, R. Saad and K. Belkacemi, *Ind. Eng. Chem. Res.*, 2007, **46**, 8806–8812.
26 J. Jang and D. S. Lee, *J. Hazard. Mater.*, 2019, **375**, 9–18.
27 Z. Cao, Y. Chen, D. Li, J. Cheng and C. Liu, *Polymers*, 2019, **11**, 253.
28 Z. Cao, P. I. Gordiichuk, K. Loos, E. J. R. Sudhölter and L. C. P. M. de Smet, *Soft Matter*, 2016, **12**, 1496–1505.
29 B. Hui, Y. Zhang and L. Ye, *Chem. Eng. J.*, 2014, **235**, 207–214.
30 Q. Liu, P. Hu, J. Wang, L. Zhang and R. Huang, *J. Taiwan Inst. Chem. Eng.*, 2016, **59**, 311–319.
31 Y. Chen, C. Liu, C. Zhang, J. Cheng, D. Wu and Z. Cao, *New Chem. Mater.*, 2020, **48**, 120–124.
32 X. Zhou, Y. Zhou, J. Nie, Z. Ji, J. Xu, X. Zhang and B. Du, *ACS Appl. Mater. Interfaces*, 2014, **6**, 4498–4513.
33 X. Zhou, J. Nie and B. Du, *ACS Appl. Mater. Interfaces*, 2017, **9**, 20913–20921.
34 X. Zhou, X. Wu, H. He, H. Liang, X. Yang, J. Nie, W. Zhang, B. Du and X. Wang, *Sens. Actuators, B*, 2020, **320**, 128328.
35 X. Zhou, F. Chen, H. Lu, L. Kong, S. Zhang, W. Zhang, J. Nie, B. Du and X. Wang, *Ind. Eng. Chem. Res.*, 2019, **58**, 10922–10930.

36 C. Sung, A. Vidyasagar, K. Hearn and J. L. Lutkenhaus, *Langmuir*, 2012, **28**, 8100–8109.
37 L. Shen, J. Fu, K. Fu, C. Picart and J. Ji, *Langmuir*, 2010, **26**, 16634–16637.
38 L. Shen, P. Chaudouet, J. Ji and C. Picart, *Biomacromolecules*, 2011, **12**, 1322–1331.
39 Y. Wu, H. Ma, D. Gu and J. a. He, *RSC Adv.*, 2015, **5**, 64520–64525.
40 Z. Cao, T. Tsoufis, T. Svaldo-Lanero, A.-S. Duwez, P. Rudolf and K. Loos, *Biomacromolecules*, 2013, **14**, 3713–3722.
41 G. Zhang, *Macromolecules*, 2004, **37**, 6553–6557.
42 T. Wang, R. Kou, J. Zhang, R. Zhu, H. Cai and G. Liu, *Langmuir*, 2020, **36**, 13051–13059.
43 B. Wan, E. J. Elzinga, R. Huang and Y. Tang, *J. Phys. Chem. C*, 2020, **124**, 28448–28457.
44 R. Funari, R. Ripa, B. Söderström, U. Skoglund and A. Q. Shen, *ACS Sens.*, 2019, **4**, 3023–3033.
45 A. G. Ayankojo, J. Reut, R. Boroznjak, A. Öpik and V. Syritski, *Sens. Actuators, B*, 2018, **258**, 766–774.
46 Z. Cao, Y. Zhang, Z. Luo, W. Li, T. Fu, W. Qiu, Z. Lai, J. Cheng, H. Yang, W. Ma, C. Liu and L. C. P. M. de Smet, *Langmuir*, 2021, **37**, 12148–12162.
47 Z. Cao, J. Guo, X. Fan, J. Xu, Z. Fan and B. Du, *Sens. Actuators, B*, 2011, **157**, 34–41.
48 J. Zhu, J. Pan, C. Ma, G. Zhang and G. Liu, *Langmuir*, 2019, **35**, 11157–11166.
49 G. Sauerbrey, *Z. Phys.*, 1959, **155**, 206–222.
50 S. M. Abdellatif Soliman, M. F. Sanad and A. E. Shalan, *RSC Adv.*, 2021, **11**, 11541–11548.
51 H. G. Schild, *Prog. Polym. Sci.*, 1992, **17**, 163–249.
52 T. Singh and R. Singhal, *J. Appl. Polym. Sci.*, 2013, **129**, 3126–3139.
53 M. Mallet, K. Barthélémy, C. Ruby, A. Renard and S. Naille, *J. Colloid Interface Sci.*, 2013, **407**, 95–101.
54 S. Vasudevan and J. Lakshmi, *RSC Adv.*, 2012, **2**, 5234–5242.